SISSA

PAPER

Simulation study of random sequential deposition of binary mixtures of lattice animals on a three-dimensional cubic lattice

View the article online for updates and enhancements.

Simulation study of random sequential deposition of binary mixtures of lattice animals on a three-dimensional cubic lattice

M Beljin-Čavić[1], I Lončarević[1,*], Lj Budinski-Petković[1], Z M Jakšić[2] and S B Vrhovac[2]

[1] Faculty of Technical Sciences, University of Novi Sad, Trg D. Obradovića 6, Novi Sad 21000, Serbia
[2] Scientific Computing Laboratory, Center for the Study of Complex Systems, Institute of Physics Belgrade, University of Belgrade, Pregrevica 118, Zemun 11080, Belgrade, Serbia
E-mail: vrhovac@ipb.ac.rs and http://ipb.ac.rs/~vrhovac/

Abstract. Random sequential adsorption of mixtures of objects of various shapes on a three-dimensional (3D) cubic lattice is studied numerically by means of Monte Carlo simulations. Depositing objects are 'lattice animals', made of a certain number of nearest neighbor sites on a lattice. We analyzed binary mixtures composed of shapes of equal size, $n = 3$, 4, 5. We concentrate here on the influence of geometrical properties of the shapes on the jamming coverage θ_J and on the temporal evolution of the density $\theta(t)$. The approach of the coverage $\theta(t)$ to the jamming limit θ_J is found to be exponential, $\theta_J - \theta(t) \sim \exp(-t/\sigma)$, both for the mixtures and their components. The values of the relaxation time σ are determined by the number of different orientations m that lattice animals can take when placed on a cubic lattice. The value of the relaxation time σ for a mixture is approximately twice the relaxation time for the pure component shape with a larger number m of possible orientations. Depending on the local

*Author to whom any correspondence should be addressed.

geometry of the objects making the mixture, the jamming coverage of a mixture θ_J can be either greater than both single-component jamming coverages or it can be in between these values. The first case is the most common, while in the second case, the jamming density of the mixture is very close to the higher jamming density for the pure component shapes. For a majority of the investigated mixtures, a component with a larger number of orientations m has a larger value of the fractional jamming density.

Keywords: classical Monte Carlo simulations

Contents
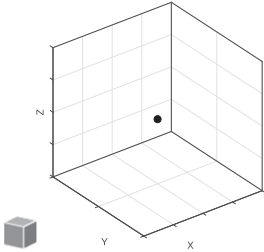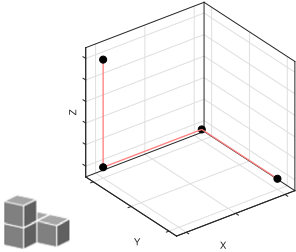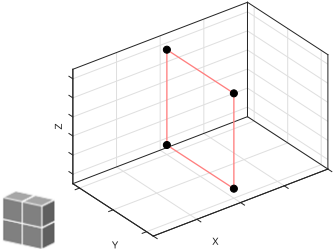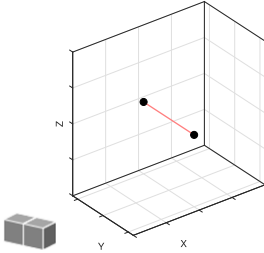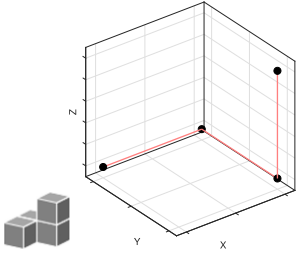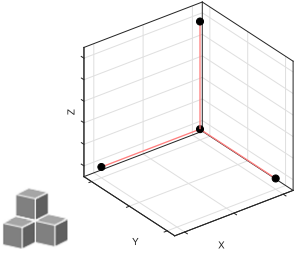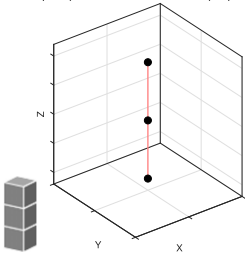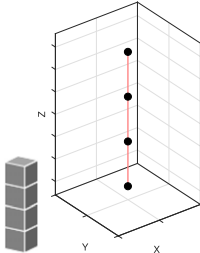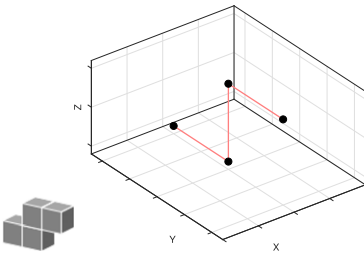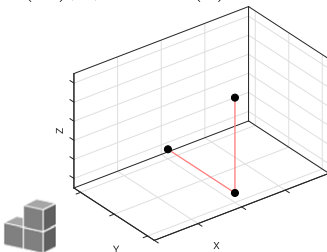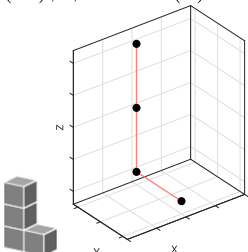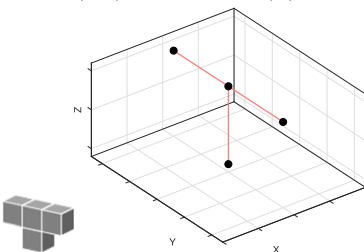
1. Introduction

Understanding the dense packings of hard particles has yielded essential insights into the structure of materials [1–3], granular media [4–7], biology [8–10], and mathematics [11–13]. Describing the packing processes is among the most persistent problems in science. For example, an issue that has been of great scientific interest for centuries is the determination of the densest arrangements of particles that do not tile space. The fact that the proof of Kepler's conjecture had not been found until 1998 [13] confirms the non-triviality of this problem. Overall, due to the enormous combinatorial problems that such systems pose, the packing structure can still not be predicted by a general model that considers controlling parameters, such as the geometric and material properties of objects, packing methods, and gravity.

The random sequential adsorption (RSA) procedure, which is the focus of the present paper, is a time-dependent process for generating nonequilibrium packings of nonoverlapping particles [14]. The RSA model represents the simplest, but non-trivial model of random packing [15]. It is very useful for studying the structure of low-temperature phases of matter, as well as particle aggregation and jamming in a wide variety of systems, from granular media [16, 17] to heterogeneous materials [18–20] and biological systems [21, 22].
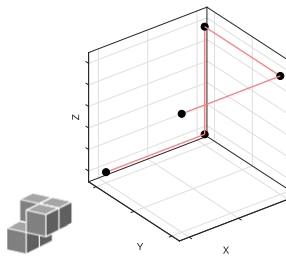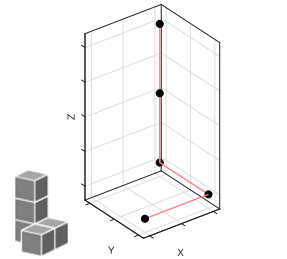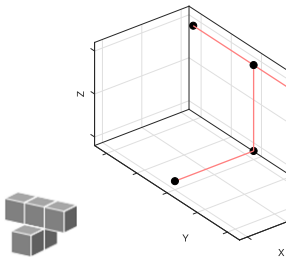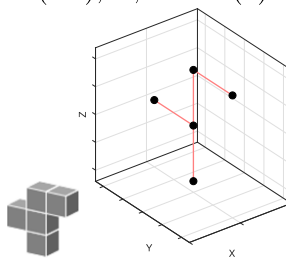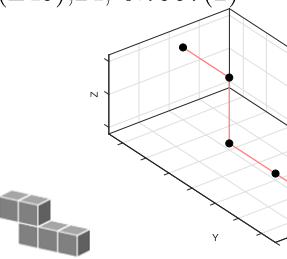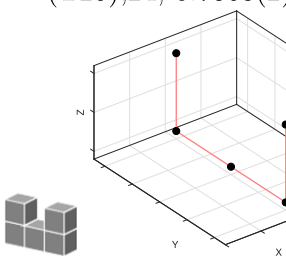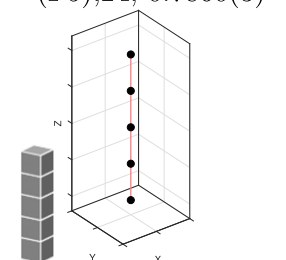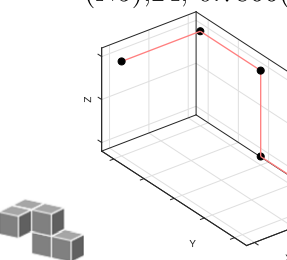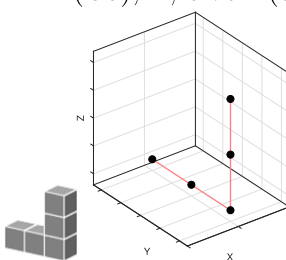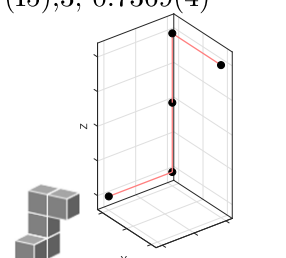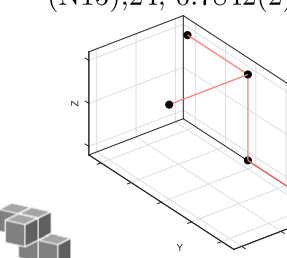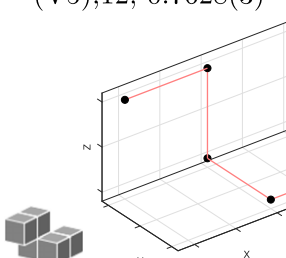
Table 1. All polycubes of size $n = 1$, 2, 3, 4 together with the equivalent lattice animals (x) on the dual lattice. For each lattice animal (x) with m possible orientations, $\theta_{\mathrm{J}}^{(x)}$ is the jamming coverage [45]. The numbers in parentheses are the numerical values of the standard uncertainty of $\theta_{\mathrm{J}}^{(x)}$ referring to the last digits of the quoted values.

(x), m; $\theta_{\mathrm{J}}^{(x)}$	(x), m; $\theta_{\mathrm{J}}^{(x)}$	(x), m; $\theta_{\mathrm{J}}^{(x)}$
(M),1; 1.0000(0)	(A4),12; 0.8178(2)	(O4),3; 0.8079(3)
(D),3; 0.9184(1)	(B4),12; 0.8178(2)	(P4),8; 0.7941(3)
(I3),3; 0.8390(2)	(I4),3; 0.7808(3)	(S4),12; 0.8149(2)
(V3),12; 0.8788(2)	(L4),24; 0.8339(2)	(T4),12; 0.8114(3)
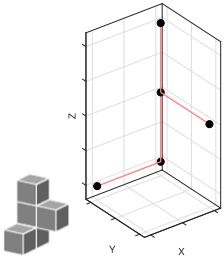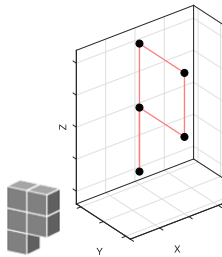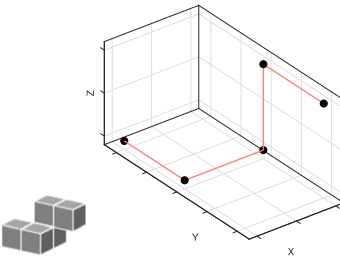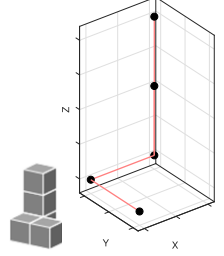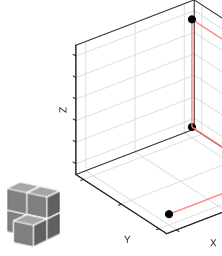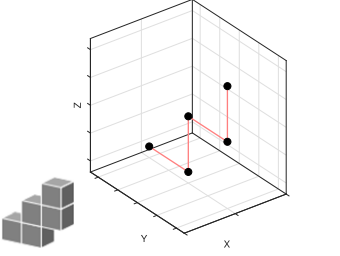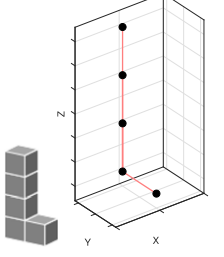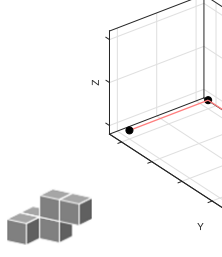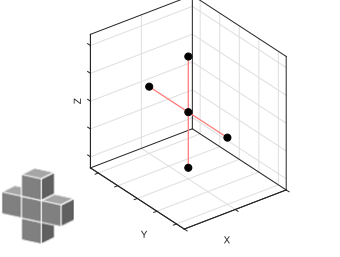
Table 2. All polycubes of size $n = 5$ together with the equivalent lattice animals (x) on the dual lattice. For each lattice animal (x) with m possible orientations, $\theta_{\mathrm{J}}^{(x)}$ is the jamming coverage [45]. The numbers in parentheses are the numerical values of the standard uncertainty of $\theta_{\mathrm{J}}^{(x)}$ referring to the last digits of the quoted values.

(x), m; $\theta_{\mathrm{J}}^{(x)}$	(x), m; $\theta_{\mathrm{J}}^{(x)}$	(x), m; $\theta_{\mathrm{J}}^{(x)}$
(A5),24; 0.7716(2)	(L45),24; 0.7957(2)	(T25),24; 0.7863(2)
(F5),24; 0.7860(3)	(N5),24; 0.7866(3)	(U5),12; 0.7611(3)
(I5),3; 0.7369(4)	(N15),24; 0.7842(2)	(V5),12; 0.7628(3)
(J15),12; 0.7635(2)	(N25),24; 0.7790(3)	(V15),12; 0.7647(3)

Table 2. Continued
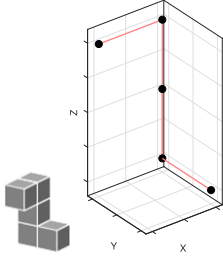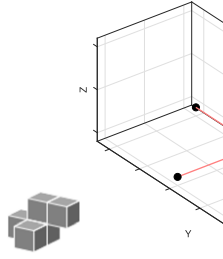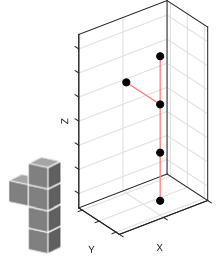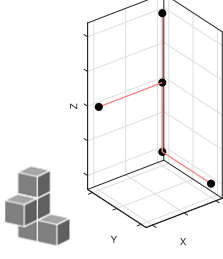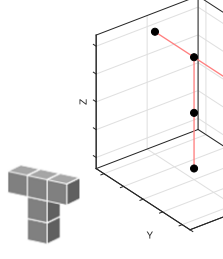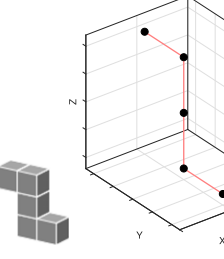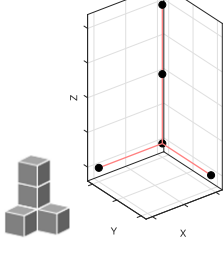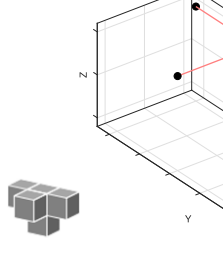
$(x), m; \theta_J^{(x)}$	$(x), m; \theta_J^{(x)}$	$(x), m; \theta_J^{(x)}$

(J25),24; 0.7839(2) (P5),24; 0.8017(3) (V25),12; 0.7647(3)

(J45),24; 0.7958(3) (Q5),24; 0.7826(3) (W5),12; 0.7615(3)

(L5),24; 0.7695(3) (S15),24; 0.7841(2) (X5),3; 0.7007(3)

The RSA model considers the sequential addition of particles of various shapes at randomly chosen places on the n-dimensional volume, subject to a nonoverlap constraint. If a new particle does not overlap with any existing particles, it will be added to the configuration; otherwise, the attempt is discarded. The time evolution of the density of the system, $\theta(t)$, i.e. the fraction of the volume occupied by the deposited objects at time t, describes the kinetic properties of the deposition process. Once an object is placed, it affects the geometry of all later placements, so that the dominant effect in RSA is the blocking of the available substrate space. At sufficiently large times, the coverage $\theta(t)$ approaches the jamming value θ_J, where only gaps that are too small to place new particles are left on the substrate.

An important property of the RSA is the adsorption kinetics in the later times of the process, which typically exhibit a very slow approach to the saturation limit $\theta(t)$. For the discrete case, the approach of the density $\theta(t)$ to the jamming limit θ_J is of the

Table 2. Continued

(x), m; $\theta_{\mathrm{J}}^{(x)}$	(x), m; $\theta_{\mathrm{J}}^{(x)}$	(x), m; $\theta_{\mathrm{J}}^{(x)}$
(L15),12; 0.7635(3)	(S25),24; 0.7790(3)	(Y5),24; 0.7595(3)
(L25),24; 0.7839(2)	(T5),12; 0.7500(3)	(Z5),12; 0.7643(2)
(L35),24; 0.7774(3)	(T15),12; 0.7582(3)	

form [23–26]:

$$\theta_{\mathrm{J}} - \theta(t) \sim \exp(-t/\sigma), \tag{1}$$

where the jamming density θ_{J} and the characteristic time σ are the parameters that depend on the details of the model, such as the shape and symmetry properties of the depositing objects [24–26].

The RSA of many different geometric objects has been studied both for continuum and lattice models in order to determine the significance of particle shape in formation of the jammed-state packings. The RSA packing process on continuous substrates has been investigated for spherical particles [27–29] and other particle shapes, including lines and ellipses [30, 31], rectangles [32, 33], starlike particles [34], superdisks bounded by the Lame curves [35], spherocylinders and ellipsoids [30, 36], cubes [37], cuboids [38], and polymers modeled as chains of identical spheres [39]. It was found that the kinetics of irreversible deposition and morphological characteristics of the packing are

strongly dependent on the shape and size of the depositing particles. Formation of random deposits on discrete substrates has also been extensively studied for various lattices and object shapes [23–26, 40–44]. Deposition of objects of various sizes and rotational symmetries that can be made by self-avoiding random walks on a square and triangular lattice was studied in [24–26]. It was found that shapes with the symmetry axis of a higher order have lower values of σ (equation (1)), i.e. they approach their jamming limit more rapidly.

Recently, we have carried out extensive numerical simulations of the random deposition of large collections of objects made by connected sites on a simple three-dimensional (3D) cubic lattice, the so-called 'lattice animals' [45]. A *lattice animal* is a finite set of nearest neighbor sites on a lattice. Object size is the number n of nodes that a lattice animal covers on the grid. We have found that the number of different orientations that lattice animals can take when placed on a cubic lattice exerts a decisive influence on the adsorption kinetics near the jamming limit θ_J. The results also suggested no correlation between the number of possible orientations of the object and the corresponding values of the jamming density θ_J.

In this paper, we present the results of Monte Carlo simulations for the irreversible RSA of mixtures of lattice animals on a 3D cubic lattice. We will concentrate on the case of binary mixtures, composed of the shapes of equal size. The binary mixture is the simplest and the first step towards the understanding of polydisperse systems. The number of examined lattice animals that make the mixtures (see tables 1 and 2) represents a good basis for studying the impact of the geometrical properties of the shapes on the jamming coverage θ_J and on the temporal evolution of the density $\theta(t)$. In general, the RSA of lattice animals on 3D lattices is a complex problem and it is difficult to develop even a qualitative understanding of the effects of shape on the packing density. Combinations of various objects increase the diversity of behaviors, so the deposition of mixtures of lattice animals is even more complicated to analyze. The aim of this work is to investigate these processes in a systematic way.

The paper is organized as follows. Section 2 describes the model and the details of the simulations. The approach of the coverage fraction $\theta(t)$ to the jamming limit θ_J is analyzed in section 3.1. The jamming densities and the jamming configurations are analyzed in section 3.2. Finally, section 4 contains some additional comments.

2. Definition of the model and the simulation method

All of the shapes studied here are *lattice animals*. Lattice animal can be viewed as a finite set of lattice sites connected by a network of bonds between nearest neighbor sites. In literature, the other relevant terms such as 'polyomino' and 'polycube' are frequently used instead the term 'lattice animal'. Polyomino of size n is an edge-connected set of n squares on the planar square lattice. A polycube of size n is a face-connected set of n cubes in the simple-cubic lattice. Because the square (cubic) lattice is self-dual, polyominoes (polycubes) are equivalent to site animals on the dual lattice, i.e. the number of polyominoes (polycubes) with n cells is precisely the number of 2D (3D) site animals with n vertices.

It is usual to differentiate between *free animals* in which two clusters that can be derived from one another by a symmetry operation of the lattice are regarded as identical, and *fixed animals* in which they are regarded as different. In other words, free lattice animals are distinguished only by shape, not by orientation. Fixed lattice animals, on the other hand, are considered distinct if they have different shapes or orientations.

In physical applications to lattice statistics, investigations are usually concerned with fixed animals. Such site animals are often called clusters, due to their close relationship to percolation problems [46, 47]. Series expansions for the percolation probability or the average cluster size can be obtained as weighted sums over the number of lattice animals $g(n, p)$, enumerated according to their size n and perimeter p [48]. In the mathematical literature, fixed polycubes are most discussed in the context of simple combinatorial problem—enumeration. The number of fixed d-dimensional polycubes of size n is usually denoted in the literature by $A_d(n)$. Lunnon [49] has made the first successful enumeration. He computed the number of polyominoes $A_2(n)$ up to size $n <= 18$. It is very interesting that to this day there is no known analytic formula for $A_d(n)$ $(d > 1)$. The only known methods for computing $A_d(n)$ are based on explicitly or implicitly enumerating all the polyominoes or polycubes using efficient numerical algorithms [49–53].

In this work, we solely consider the free lattice animals on a 3D cubic lattice (the term 'free' is omitted in the following text). Lunnon [54] analyzed polycubes by considering symmetry groups and computed the number of three-dimensional polycubes of size up to $n = 6$. Most polycubes are asymmetric, but many have more complex symmetry groups. A polycube without symmetry has 24 different orientations. It is evident that a number of orientations that a polycube may take varies with the symmetry of the polycube.

Table 1 shows all polycubes of size $n = 1, 2, 3$, and 4 and equivalent lattice animals on the dual lattice. Polycubes of size $n = 1, 2, 3$ are planar with a maximum of twelve different orientations (object V3). There are eight tetracubes (fourth-order polycubes), five of which are planar [55]. A tetracube A4 and its mirror image B4 (chiral twins) are considered distinct because there is no rigid motion that transforms one onto the other.

All polycubes of size $n = 5$ (pentacubes) are shown in table 2 together with equivalent lattice animals on the dual lattice. There are 29 distinct three-dimensional pentacubes [55]. Twelve pentacubes are flat (pentominoes). Among the nonplanar pentacubes, there are five that have at least one plane of symmetry (A5, L35, Q5, T15, T25) and each of them is its own mirror image. The remaining twelve nonplanar pentacubes form six chiral pairs: J15–L15, J25–L25, J45–L45, N15–S15, N25–S25, V15–V25. Of the 29 pentacubes, for two flats (I5, X5) there are only three possible orientations. Ten pentacubes have twelve orientations and each of the remaining 17 pentacubes has 24 orientations.

Table 3 shows the number of possible orientations m for polycubes of size $n \leqslant 6$ and the number of objects $A_3^m(n)$ with the specified number of orientations. Polycubes of size $n \leqslant 5$ can have 1, 3, 8, 12 or 24 different orientations. It is interesting that among the polycubes of size $n \leqslant 6$ only one object has eight different orientations (see tetracube P4 in table 1). However, there are hexacubes (sixth-order polycubes) that have four and six different orientation [45, 55].

Table 3. The number of polycubes $A_3^m(n)$ of size n with the specified number of possible orientations $m = 1, 3, 4, 6, 8, 12, 24$. The results are shown for all polycubes of size $n \leqslant 6$.

	A_3^1	A_3^3	A_3^4	A_3^6	A_3^8	A_3^{12}	A_3^{24}	$N = \sum_m A_3^m$
$n = 1$	1							1
$n = 2$		1						1
$n = 3$		1				1		2
$n = 4$		2			1	4	1	8
$n = 5$		2				10	17	29
$n = 6$		1	1	3		34	127	166

Numerical values of the jamming densities θ_J for all lattice animals of size $n \leqslant 5$ are given in tables 1 and 2 [45]. It is evident that jamming densities θ_J decrease rapidly with the size n of the objects. Most objects of size $n \leqslant 4$ have a jamming density θ_J greater than 0.80, while θ_J for all objects of size $n = 5$ is in the interval 0.70–0.80. The noticeable drop in the jamming density θ_J is thus a clear consequence of the enhanced frustration of the spatial adsorption. As expected, in each chiral pair both objects have the identical values of the jamming density.

2.1. Simulation method

The numerical algorithm used to deposit a lattice animal at randomly chosen places on the 3D substrate was already described in detail in the previous paper [45]. Therefore, we shall present it briefly, giving the algorithm additions necessary for the random deposition of the two types of objects (binary mixture).

The primary lattice animal is a connected set of sites in the cubic lattice that contains the origin $(0, 0, 0)$. We call that point the head of an object. In the case of mixtures, at each Monte Carlo step, a lattice site and one of the primary objects that make the mixture are selected at random. If the selected site is unoccupied, deposition of the chosen object is tried in one of the 24 orientations, which is chosen at random. Then we fix the head of the object at the selected site and search whether all necessary sites are unoccupied. If so, we occupy these sites and place the object. If the attempt fails, a new site, a new primary object, and a new orientation are selected at random, and so on. The numerical algorithm that provides a search of all possible object orientations and selecting the random orientation of a lattice animal is given in the previous paper [45]. We have verified that usage of different heads for all examined objects quantitatively gives the same results for the temporal evolution of density $\theta(t)$ and the jamming limit θ_J.

During the simulation, we can record the number of all inaccessible sites in the lattice. These include the occupied sites and the sites that are unoccupied but cannot be the head of the object deposited in any of the 24 possible orientations. The jamming limit is reached when the number of inaccessible sites is equal to the total number of sites in the lattice. Checking this condition is performed after every kL^3 attempts to absorb the object, starting at some late time point estimated in the trial simulations

Table 4. Jamming coverages $\theta_{\mathrm{J}}^{(\mathrm{mix})}$ of mixtures I4 + I6 and V5 + J15, obtained in simulations for lattices of size $L = 64, 96, 128$. The numbers in parentheses are the numerical values of the standard uncertainty of $\theta_{\mathrm{J}}^{(\mathrm{mix})}$ referring to the last digits of the quoted values.

L	(I4) + (I6)	(V5) + (J15)
64	0.7951(4)	0.7836(4)
96	0.7952(4)	0.7834(4)
128	0.7952(3)	0.7834(3)

on smaller lattices. Depending on the objects size, the values of parameter k are 5, 20, and 50. If the condition is true, we stop the current run and continue with the next simulation run.

The Monte Carlo simulations are performed on a 3D cubic lattice of size $L = 128$. Periodic boundary conditions are used in all directions. The time is counted by the number of attempts to select a lattice site and scaled by the total number of lattice sites $L^3 \approx 2$ million. The data are averaged over 128 independent runs for each of the investigated binary mixtures.

In order to obtain assessments of finite-size effects, different lattice sizes have been used. We have chosen binary mixtures I4 + I6 and V5 + J15 and performed the simulations for lattices of size $L = 64, 96, 128$ (see table 4). These simulations suggest that the numerically obtained jamming densities averaged over 128 trials on the lattices of size $L = 128$ are precise within four significant digits.

3. Results and discussion

Using the RSA algorithm defined in the preceding section, extensive calculations were performed in order to determine the time evolution of the density $\theta(t)$ and the structure of the 3D deposit. Binary mixtures of lattice animals used in our simulations are made of various shapes from tables 1 and 2, covering $n = 3, 4$, and 5 lattice sites.

For $n = 3$ and 4 all possible combinations of lattice animals are examined and the results are presented in tables 5–7. Mixtures of $n = 5$ size objects are made for all combinations of twelve chosen shapes: I5, J15, L5, L15, L35, L45, T5, T25, V5, X5, Y5, and Z5. Among them, there are seven planar and five nonplanar lattice animals. Of the 12 chosen pentacubes, two flats have three possible orientations, five have twelve orientations, and each of the remaining five pentacubes has 24 orientations. Results for these mixtures are given in tables 9–14. In addition to these mixtures of objects of the same size, simulations are performed for mixtures of k-mers of different sizes $n = 2, 4, 6, 8$ and 10 (see table 15). Besides the total jamming densities θ_{J} for mixtures, the fractional jamming densities for each component, $\theta_{\mathrm{J}}^{(x_i)}$ ($i = 1, 2$), are also included in tables 5–15.

Figure 1 shows typical snapshot configurations at the jamming density obtained for mixtures (a) B4 + L4, and (b) L45 + X5. The snapshots of size $\Delta L^3 = 10^3$ are

Table 5. For a binary mixture of lattice animals (x_1) and (x_2) of size $(n_1,\ n_2)$, with $(m_1,\ m_2)$ possible orientations (see table 1), $\theta_{\mathrm{J}}^{(x)}$ is the total jamming density, and $\theta_{\mathrm{J}}^{(x_i)}$ $(i = 1, 2)$ are the fractional jamming densities for each mixture component. The numbers in parentheses are the numerical values of the standard uncertainty of the jamming density referring to the last digits of the quoted values. Bold—planar object, roman—non-planar object.

$(x_1) + (x_2)$	n_1	n_2	m_1	m_2	$\theta_{\mathrm{J}}^{(x_1)}$	$\theta_{\mathrm{J}}^{(x_2)}$	$\theta_{\mathrm{J}}^{(x)}$
(I3) + **(V3)**	3	3	3	12	0.4248(2)	0.4664(2)	0.8912(2)
(A4) + (B4)	4	4	12	12	0.4176(2)	0.4178(2)	0.8354(2)
(A4) + **(I4)**	4	4	12	3	0.4427(2)	0.3917(2)	0.8344(2)
(A4) + **(L4)**	4	4	12	24	0.4213(2)	0.4317(2)	0.8530(2)
(A4) + **(O4)**	4	4	12	3	0.4205(2)	0.4152(2)	0.8357(2)
(A4) + (P4)	4	4	12	8	0.4244(2)	0.4049(2)	0.8293(2)
(A4) + **(S4)**	4	4	12	12	0.4189(2)	0.4169(2)	0.8358(2)
(A4) + **(T4)**	4	4	12	12	0.4230(2)	0.4142(2)	0.8372(2)

Table 6. For a binary mixture of lattice animals (x_1) and (x_2) of size $(n_1,\ n_2)$, with $(m_1,\ m_2)$ possible orientations (see table 1), $\theta_{\mathrm{J}}^{(x)}$ is the total jamming density, and $\theta_{\mathrm{J}}^{(x_i)}$ $(i = 1, 2)$ are the fractional jamming densities for each mixture component. The numbers in parentheses are the numerical values of the standard uncertainty of the jamming density referring to the last digits of the quoted values. Bold—planar object, roman—non-planar object.

$(x_1) + (x_2)$	n_1	n_2	m_1	m_2	$\theta_{\mathrm{J}}^{(x_1)}$	$\theta_{\mathrm{J}}^{(x_2)}$	$\theta_{\mathrm{J}}^{(x)}$
(B4) + **(I4)**	4	4	12	3	0.4426(2)	0.3917(2)	0.8343(2)
(B4) + **(L4)**	4	4	12	24	0.4211(2)	0.4319(2)	0.8530(2)
(B4) + **(O4)**	4	4	12	3	0.4204(2)	0.4152(2)	0.8356(2)
(B4) + (P4)	4	4	12	8	0.4244(2)	0.4048(2)	0.8292(2)
(B4) + **(S4)**	4	4	12	12	0.4189(2)	0.4168(2)	0.8357(2)
(B4) + **(T4)**	4	4	12	12	0.4230(2)	0.4142(2)	0.8372(2)
(I4) + **(L4)**	4	4	3	24	0.3898(2)	0.4560(2)	0.8458(2)
(I4) + **(O4)**	4	4	3	3	0.3925(2)	0.4358(2)	0.8283(2)
(I4) + (P4)	4	4	3	8	0.3884(2)	0.4234(2)	0.8118(2)
(I4) + **(S4)**	4	4	3	12	0.3905(2)	0.4376(2)	0.8281(2)
(I4) + **(T4)**	4	4	3	12	0.3898(2)	0.4347(2)	0.8245(2)

taken from the central part of the lattice. The first mixture is made of the objects with $m = 12(\mathrm{B4})$ and $m = 24(\mathrm{L4})$ possible orientations and the second one of the object with $m = 24(\mathrm{L45})$ and $m = 3(\mathrm{X5})$ possible orientations.

Table 7. For a binary mixture of lattice animals (x_1) and (x_2) of size (n_1, n_2), with (m_1, m_2) possible orientations (see table 1), $\theta_{\mathrm{J}}^{(x)}$ is the total jamming density, and $\theta_{\mathrm{J}}^{(x_i)}$ $(i = 1, 2)$ are the fractional jamming densities for each mixture component. The numbers in parentheses are the numerical values of the standard uncertainty of the jamming density referring to the last digits of the quoted values. Bold—planar object, roman—non-planar object.

$(x_1) + (x_2)$	n_1	n_2	m_1	m_2	$\theta_{\mathrm{J}}^{(x_1)}$	$\theta_{\mathrm{J}}^{(x_2)}$	$\theta_{\mathrm{J}}^{(x)}$
(L4) + **(O4)**	4	4	24	3	0.4376(2)	0.4225(2)	0.8601(2)
(L4) + (P4)	4	4	24	8	0.4358(2)	0.4080(2)	0.8438(2)
(L4) + **(S4)**	4	4	24	12	0.4295(2)	0.4181(2)	0.8476(2)
(L4) + **(T4)**	4	4	24	12	0.4275(2)	0.4096(2)	0.8371(2)
(O4) + (P4)	4	4	3	8	0.4106(2)	0.3981(2)	0.8087(2)
(O4) + **(S4)**	4	4	3	12	0.4134(2)	0.4150(2)	0.8284(2)
(O4) + **(T4)**	4	4	3	12	0.4163(2)	0.4142(2)	0.8305(2)
(P4) + **(S4)**	4	4	8	12	0.4050(2)	0.4245(2)	0.8295(2)
(P4) + **(T4)**	4	4	8	12	0.4137(2)	0.4222(2)	0.8359(2)
(S4) + **(T4)**	4	4	12	12	0.4210(2)	0.4179(2)	0.8389(2)

Table 8. For a binary mixture of lattice animals (x_1) and (x_2) of size (n_1, n_2), with (m_1, m_2) possible orientations (see table 2), $\theta_{\mathrm{J}}^{(x)}$ is the total jamming density, and $\theta_{\mathrm{J}}^{(x_i)}$ $(i = 1, 2)$ are the fractional jamming densities for each mixture component. The numbers in parentheses are the numerical values of the standard uncertainty of the jamming density referring to the last digits of the quoted values. Bold—planar object, roman—non-planar object.

$(x_1) + (x_2)$	n_1	n_2	m_1	m_2	$\theta_{\mathrm{J}}^{(x_1)}$	$\theta_{\mathrm{J}}^{(x_2)}$	$\theta_{\mathrm{J}}^{(x)}$
(L5) + **(I5)**	5	5	24	3	0.4225(3)	0.3644(3)	0.7869(3)
(L5) + (J15)	5	5	24	12	0.3925(2)	0.3977(2)	0.7902(2)
(L5) + (L15)	5	5	24	12	0.3925(2)	0.3977(2)	0.7902(2)
(L5) + (L35)	5	5	24	24	0.3889(3)	0.4065(3)	0.7954(3)
(L5) + (L45)	5	5	24	24	0.3901(2)	0.4207(2)	0.8108(2)
(L5) + **(T5)**	5	5	24	12	0.3978(3)	0.3865(3)	0.7843(3)
(L5) + (T25)	5	5	24	24	0.3936(2)	0.4125(2)	0.8061(2)
(L5) + (V5)	5	5	24	12	0.3968(3)	0.3953(3)	0.7921(3)
(L5) + (X5)	5	5	24	3	0.4081(3)	0.3585(3)	0.7666(3)
(L5) + (Y5)	5	5	24	24	0.3872(3)	0.3803(3)	0.7675(3)
(L5) + (Z5)	5	5	24	12	0.3932(3)	0.3977(3)	0.7909(3)

3.1. RSA kinetics

The kinetics of the irreversible deposition of mixtures are illustrated in figure 2, where the plots of $\theta_{\mathrm{J}} - \theta(t)$ and $\theta_{\mathrm{J}}^{(i)} - \theta_i(t)$, $(i = 1, 2)$ vs t are given for some combinations of the shapes from tables 1 and 2. Here, fractional jamming densities $\theta_{\mathrm{J}}^{(i)}$, $(i = 1, 2)$ are

Table 9. For a binary mixture of lattice animals (x_1) and (x_2) of size (n_1, n_2), with (m_1, m_2) possible orientations (see table 2), $\theta_{\mathrm{J}}^{(x)}$ is the total jamming density, and $\theta_{\mathrm{J}}^{(x_i)}$ $(i = 1, 2)$ are the fractional jamming densities for each mixture component. The numbers in parentheses are the numerical values of the standard uncertainty of the jamming density referring to the last digits of the quoted values. Bold—planar object, roman—non-planar object.

$(x_1) + (x_2)$	n_1	n_2	m_1	m_2	$\theta_{\mathrm{J}}^{(x_1)}$	$\theta_{\mathrm{J}}^{(x_2)}$	$\theta_{\mathrm{J}}^{(x)}$
(V5) + **(I5)**	5	5	12	3	0.4175(3)	0.3669(3)	0.7844(3)
(V5) + (J15)	5	5	12	12	0.3882(3)	0.3952(3)	0.7834(3)
(V5) + (L15)	5	5	12	12	0.3884(3)	0.3950(3)	0.7834(3)
(V5) + (L35)	5	5	12	24	0.3850(2)	0.4070(2)	0.7920(2)
(V5) + (L45)	5	5	12	24	0.3866(3)	0.4192(3)	0.8058(3)
(V5) + **(T5)**	5	5	12	12	0.3915(3)	0.3824(3)	0.7739(3)
(V5) + (T25)	5	5	12	24	0.3908(2)	0.4123(2)	0.8031(2)
(V5) + **(X5)**	5	5	12	3	0.4023(3)	0.3567(3)	0.7590(3)
(V5) + **(Y5)**	5	5	12	24	0.3944(3)	0.3893(3)	0.7837(3)
(V5) + **(Z5)**	5	5	12	12	0.3890(3)	0.3954(3)	0.7844(3)

Table 10. For a binary mixture of lattice animals (x_1) and (x_2) of size (n_1, n_2), with (m_1, m_2) possible orientations (see table 2), $\theta_{\mathrm{J}}^{(x)}$ is the total jamming density, and $\theta_{\mathrm{J}}^{(x_i)}$ $(i = 1, 2)$ are the fractional jamming densities for each mixture component. The numbers in parentheses are the numerical values of the standard uncertainty of the jamming density referring to the last digits of the quoted values. Bold—planar object, roman—non-planar object.

$(x_1) + (x_2)$	n_1	n_2	m_1	m_2	$\theta_{\mathrm{J}}^{(x_1)}$	$\theta_{\mathrm{J}}^{(x_2)}$	$\theta_{\mathrm{J}}^{(x)}$
(I5) + (J15)	5	5	3	12	0.3629(3)	0.4168(3)	0.7797(3)
(I5) + (L15)	5	5	3	12	0.3627(3)	0.4171(3)	0.7798(3)
(I5) + (L35)	5	5	3	24	0.3587(2)	0.4270(2)	0.7857(2)
(I5) + (L45)	5	5	3	24	0.3635(2)	0.4461(2)	0.8096(2)
(I5) + **(T5)**	5	5	3	12	0.3664(3)	0.4067(3)	0.7731(3)
(I5) + (T25)	5	5	3	24	0.3635(3)	0.4375(3)	0.8010(3)
(I5) + **(X5)**	5	5	3	3	0.3668(3)	0.3668(3)	0.7336(3)
(I5) + **(Y5)**	5	5	3	24	0.3639(3)	0.4152(3)	0.7791(3)
(I5) + **(Z5)**	5	5	3	12	0.3632(3)	0.4159(3)	0.7791(3)

densities of the components making the mixture in the jamming state of mixture. These plots are straight lines on a logarithmic scale for the late times of deposition, suggesting that in the case of mixtures the approach to the jamming limit is also exponential (1) both for the mixtures and their components.

In [45], it was pointed out that the relaxation time σ (equation (1)) for the single-object deposition is approximately equal to the number of different orientations m that lattice animals can take when placed on a cubic lattice. There are seven classes of lattice

Table 11. For a binary mixture of lattice animals (x_1) and (x_2) of size $(n_1,\ n_2)$, with $(m_1,\ m_2)$ possible orientations (see table 2), $\theta_{\mathrm{J}}^{(x)}$ is the total jamming density, and $\theta_{\mathrm{J}}^{(x_i)}$ $(i = 1, 2)$ are the fractional jamming densities for each mixture component. The numbers in parentheses are the numerical values of the standard uncertainty of the jamming density referring to the last digits of the quoted values. Bold—planar object, roman—non-planar object.

$(x_1) + (x_2)$	n_1	n_2	m_1	m_2	$\theta_{\mathrm{J}}^{(x_1)}$	$\theta_{\mathrm{J}}^{(x_2)}$	$\theta_{\mathrm{J}}^{(x)}$
(J15) + (L15)	5	5	12	12	0.3935(2)	0.3935(2)	0.7870(2)
(J15) + (L35)	5	5	12	24	0.3901(2)	0.4009(2)	0.7910(2)
(J15) + (L45)	5	5	12	24	0.3894(3)	0.4135(3)	0.8029(3)
(J15) + **(T5)**	5	5	12	12	0.3971(2)	0.3809(2)	0.7780(2)
(J15) + (T25)	5	5	12	24	0.3939(3)	0.4069(3)	0.8008(3)
(J15) + **(X5)**	5	5	12	3	0.4146(3)	0.3571(3)	0.7717(3)
(J15) + **(Y5)**	5	5	12	24	0.3997(3)	0.3873(3)	0.7870(3)
(J15) + **(Z5)**	5	5	12	12	0.3928(2)	0.3934(2)	0.7862(2)

Table 12. For a binary mixture of lattice animals (x_1) and (x_2) of size $(n_1,\ n_2)$, with $(m_1,\ m_2)$ possible orientations (see table 2), $\theta_{\mathrm{J}}^{(x)}$ is the total jamming density, and $\theta_{\mathrm{J}}^{(x_i)}$ $(i = 1, 2)$ are the fractional jamming densities for each mixture component. The numbers in parentheses are the numerical values of the standard uncertainty of the jamming density referring to the last digits of the quoted values. Bold—planar object, roman—non-planar object.

$(x_1) + (x_2)$	n_1	n_2	m_1	m_2	$\theta_{\mathrm{J}}^{(x_1)}$	$\theta_{\mathrm{J}}^{(x_2)}$	$\theta_{\mathrm{J}}^{(x)}$
(L15) + (L35)	5	5	12	24	0.3900(3)	0.4010(3)	0.7910(3)
(L15) + (L45)	5	5	12	24	0.3884(3)	0.4127(3)	0.8011(3)
(L15) + **(T5)**	5	5	12	12	0.3970(3)	0.3810(3)	0.7780(3)
(L15) + (T25)	5	5	12	24	0.3939(2)	0.4069(2)	0.8008(2)
(L15) + **(X5)**	5	5	12	3	0.4144(2)	0.3572(2)	0.7716(2)
(L15) + **(Y5)**	5	5	12	24	0.3996(3)	0.3874(3)	0.7870(3)
(L15) + **(Z5)**	5	5	12	12	0.3928(2)	0.3933(2)	0.7861(2)

animals with different numbers of possible orientations on a cubic lattice, and the corresponding values of the parameter σ are $\sigma \simeq m \in \{1, 3, 4, 6, 8, 12, 24\}$ [45]. The kinetics of the process are examined for a large number of mixtures comprising all combinations of numbers of possible orientations of the mixture components. For the illustration, in figure 2 kinetics are presented for the two-component mixtures of objects with $(m = 3,\ m = 12)$, $(m = 12,\ m = 24)$, $(m = 12,\ m = 8)$, and $(m = 12,\ m = 12)$ possible orientations. In the case of mixtures, the rapidity of the approach to the jamming limit is determined by the component shape with a larger number of possible orientations m. The value of the relaxation time σ for a mixture is approximately twice the relaxation time for the pure component shape with a larger number m of possible orientations.

Table 13. For a binary mixture of lattice animals (x_1) and (x_2) of size (n_1, n_2), with (m_1, m_2) possible orientations (see table 2), $\theta_J^{(x)}$ is the total jamming density, and $\theta_J^{(x_i)}$ $(i = 1, 2)$ are the fractional jamming densities for each mixture component. The numbers in parentheses are the numerical values of the standard uncertainty of the jamming density referring to the last digits of the quoted values. Bold—planar object, roman—non-planar object.

$(x_1) + (x_2)$	n_1	n_2	m_1	m_2	$\theta_J^{(x_1)}$	$\theta_J^{(x_2)}$	$\theta_J^{(x)}$
(L35) + (L45)	5	5	24	24	0.3952(3)	0.4091(3)	0.8043(3)
(L35) + **(T5)**	5	5	24	12	0.4108(2)	0.3795(2)	0.7903(2)
(L35) + (T25)	5	5	24	24	0.4028(3)	0.4051(3)	0.8079(3)
(L35) + **(X5)**	5	5	24	3	0.4306(3)	0.3562(3)	0.7868(3)
(L35) + **(Y5)**	5	5	24	24	0.4104(3)	0.3850(3)	0.7954(3)
(L35) + **(Z5)**	5	5	24	12	0.4005(3)	0.3899(3)	0.7904(3)
(L45) + **(T5)**	5	5	24	12	0.4212(3)	0.3794(3)	0.8006(3)
(L45) + (T25)	5	5	24	24	0.4124(3)	0.3996(3)	0.8120(3)
(L45) + **(X5)**	5	5	24	3	0.4377(3)	0.3556(3)	0.7933(3)
(L45) + **(Y5)**	5	5	24	24	0.4213(2)	0.3840(2)	0.8053(2)
(L45) + **(Z5)**	5	5	24	12	0.4136(2)	0.3898(2)	0.8034(2)

Table 14. For a binary mixture of lattice animals (x_1) and (x_2) of size (n_1, n_2), with (m_1, m_2) possible orientations (see table 2), $\theta_J^{(x)}$ is the total jamming density, and $\theta_J^{(x_i)}$ $(i = 1, 2)$ are the fractional jamming densities for each mixture component. The numbers in parentheses are the numerical values of the standard uncertainty of the jamming density referring to the last digits of the quoted values. Bold—planar object, roman—non-planar object.

$(x_1) + (x_2)$	n_1	n_2	m_1	m_2	$\theta_J^{(x_1)}$	$\theta_J^{(x_2)}$	$\theta_J^{(x)}$
(T5) + (T25)	5	5	12	24	0.3845(2)	0.4135(2)	0.7980(2)
(T5) + **(X5)**	5	5	12	3	0.3996(3)	0.3573(3)	0.7569(3)
(T5) + **(Y5)**	5	5	12	24	0.3876(2)	0.3917(2)	0.7793(2)
(T5) + **(Z5)**	5	5	12	12	0.3818(2)	0.3977(2)	0.7795(2)
(T25) + **(X5)**	5	5	24	3	0.4295(3)	0.3543(3)	0.7838(3)
(T25) + **(Y5)**	5	5	24	24	0.4123(2)	0.3875(2)	0.7998(2)
(T25) + **(Z5)**	5	5	24	12	0.4065(2)	0.3953(2)	0.8018(2)
(X5) + **(Y5)**	5	5	3	24	0.3584(3)	0.4057(3)	0.7641(3)
(X5) + **(Z5)**	5	5	3	12	0.3573(3)	0.4122(3)	0.7695(3)
(Y5) + **(Z5)**	5	5	24	12	0.3877(3)	0.3992(3)	0.7869(3)

At large times, deposition events take place on clusters of unoccupied sites. There is only a restricted number of possible orientations in which a component shape can reach a vacant location, provided the location is small enough. Namely, for a component shape with a larger number of possible placements, a longer time is needed to examine all isolated empty locations that are left in the late times of the deposition process. The

Table 15. For a binary mixture of k-mers In_1 and In_2 of size (n_1, n_2), with $m_1 = m_2 = 3$ possible orientations, $\theta_J^{(x)}$ is the total jamming density, and $\theta_J^{(x_i)}$ $(i = 1, 2)$ are the fractional jamming densities for each mixture component. The numbers in parentheses are the numerical values of the standard uncertainty of the jamming density referring to the last digits of the quoted values. All objects are planar.

$(x_1) + (x_2)$	n_1	n_2	m_1	m_2	$\theta_J^{(x_1)}$	$\theta_J^{(x_2)}$	$\theta_J^{(x)}$
(I2) + (I10)	2	10	3	3	0.6960(2)	0.2309(2)	0.9269(2)
(I2) + (I4)	2	4	3	3	0.5839(1)	0.3422(1)	0.9261(1)
(I2) + (I6)	2	6	3	3	0.6385(2)	0.2887(2)	0.9272(2)
(I2) + (I8)	2	8	3	3	0.6723(2)	0.2549(2)	0.9272(2)
(I4) + (I10)	4	10	3	3	0.5829(4)	0.2155(4)	0.7984(4)
(I4) + (I6)	4	6	3	3	0.5023(3)	0.2929(3)	0.7952(3)
(I4) + (I8)	4	8	3	3	0.5518(3)	0.2456(3)	0.7974(3)
(I6) + (I10)	6	10	3	3	0.4935(5)	0.2283(5)	0.7218(5)
(I6) + (I8)	6	8	3	3	0.4470(5)	0.2711(5)	0.7181(5)
(I8) + (I10)	8	10	3	3	0.4091(6)	0.2584(6)	0.6675(6)

increase in the number of possible shape placements extends the mean waiting time between consecutive and successful deposition events. Consequently, the approach to the jamming state is slower for the component shape with a larger value of parameter m. If we imagine a cluster of unoccupied sites such that deposition of component shape (x) is possible, prior to a successful (x)-shape deposition there will probably be some rejected attempts of (y)-component shape deposition. Therefore, the overall process near jamming density will proceed more slowly than each of the individual deposition processes.

3.2. Jamming densities

The following conclusions can be drawn from the results given in tables 5–15. At first, the jamming density for the mixture I3 + V3 of objects covering three lattice sites has a larger value than either of the jamming densities for components. Similarly, in the case of two-component mixtures of different objects covering four lattice sites, mixtures always fill the lattice more efficiently than the single objects making the mixture. Analyzing the results from tables 5–7 it can be noted that object L4 has the best packing facilities with other objects. However, there are a small number of exceptions to this rule: $\theta_J(\text{T4} + \text{S4}) > \theta_J(\text{T4} + \text{L4})$, $\theta_J(\text{T4} + \text{A4}) \gtrsim \theta_J(\text{T4} + \text{L4})$, and $\theta_J(\text{T4} + \text{B4}) \gtrsim \theta_J(\text{T4} + \text{L4})$. On the contrary, object P4 gives the lowest packing densities when combined with other objects of the same size. Also, in this case, there are a small number of exceptions: $\theta_J(\text{L4} + \text{T4}) < \theta_J(\text{L4} + \text{P4})$, $\theta_J(\text{S4} + \text{O4}) < \theta_J(\text{S4} + \text{P4})$, and $\theta_J(\text{S4} + \text{I4}) < \theta_J(\text{S4} + \text{P4})$. These exceptions show the complexity of the problem of 3D random packing of mixtures of various shapes.

The number of different shapes grows sharply with the object size and for larger objects it is practically impossible to investigate all of the combinations. We have chosen twelve characteristic shapes of size $n = 5$ and performed the simulations for all
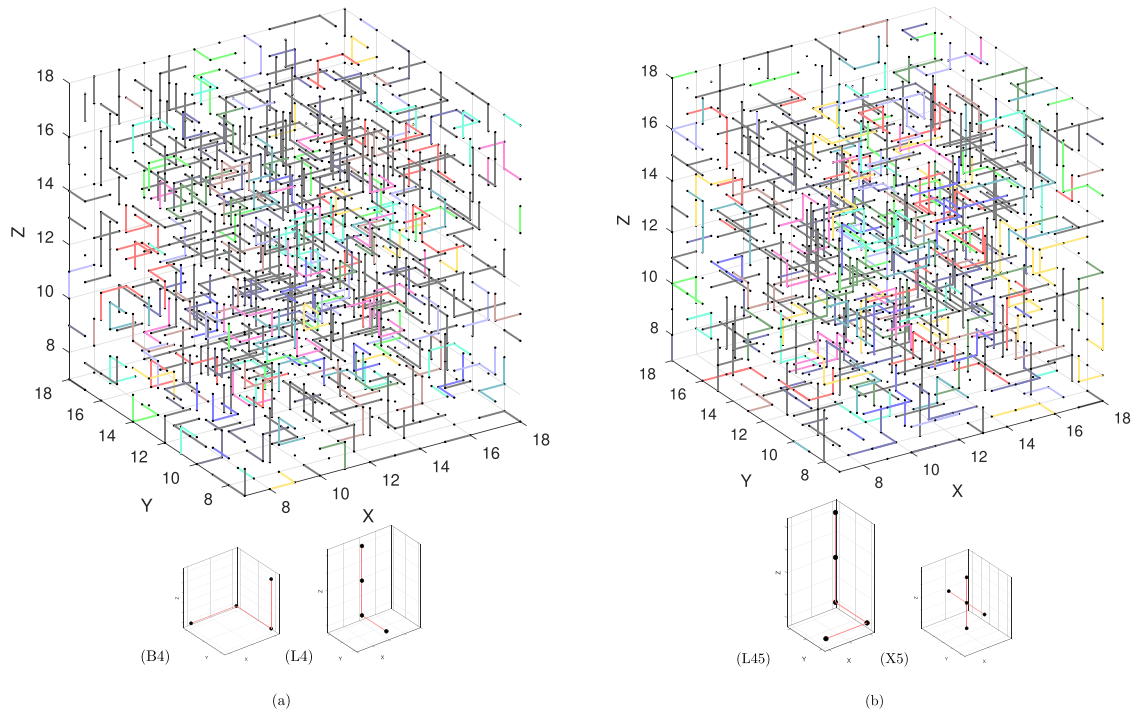
Figure 1. Snapshots of patterns formed during the RSA of mixtures (a) B4($m = 12$) + L4($m = 24$), (table 1); (b) L45($m = 24$) + X5($m = 3$), (table 2); the snapshots are taken from the central part of the lattice at times needed for the system to reach the jamming state. The corresponding lattice animals are shown below both (a) and (b). The objects B4 and L45 are colored with twelve colors randomly selected for each one. Objects L4 and X5 are painted black.

possible binary mixtures containing these objects (see tables 8–14). The results of these simulations suggest that the jamming limit almost always has larger values for mixtures than for the single objects making the mixture. There are only four exceptions among the examined combinations: (V5, X5), (L5, X5), (L5, Y5) and (I5, X5).

Objects L45 gives the largest values of jamming densities combined with other examined objects, except with the object L35: $\theta_J(L35 + L45) < \theta_J(L35 + T25)$. Binary mixtures with object T25 as a component also have high jamming density values. Accordingly, mixture L45 + T25 has the highest jamming density $\theta_J(L45 + T25) = 0.8120(3)$ among all analyzed ones. The results of numerical simulations show that the object X5, combined with other considered shapes, causes the lowest jamming limits.

Mixtures of objects of various sizes are made combining k-mers of various lengths. From table 15 it can be seen that the jamming density for a mixture of k-mers of two different lengths is always larger than θ_J for either of the components. These results are in qualitative agreement with the results presented in [56] for mixtures of k-mers on a square lattice.

Fractional jamming densities of the mixture components are also analyzed. The results for the examined mixtures suggest that the fraction of a k-mer in a mixture is always lower than the fraction of other component of the same size. It is interesting that
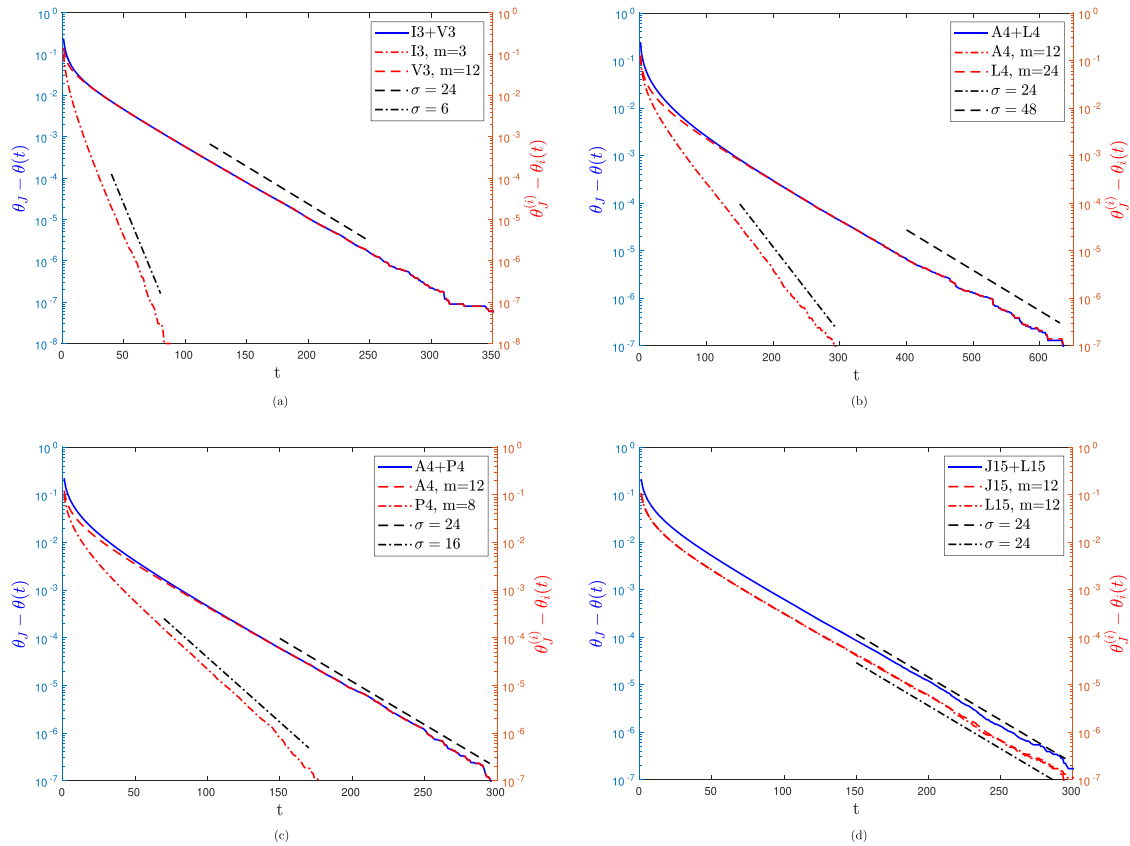
Figure 2. Plots of $\theta_J - \theta(t)$ (left-hand axis) and $\theta_J^{(i)} - \theta_i(t)$, $i = 1, 2$ (right-hand axis) versus t for mixtures: (a) I3($m = 3$) + V3($m = 12$), (b) A4($m = 12$) + L4 ($m = 24$), (c) A4($m = 12$) + P4($m = 8$), (d) J15($m = 12$) + L15($m = 12$). Additionally, the slanted straight lines with the slopes $-1/\sigma$, $\sigma = 2m$ are shown, indicating the late-time RSA behavior and are guide to the eye.

in the mixture of k-mer I5 and object X5, both components have the same fractional density. Mixture I5 + X5 has the lowest jamming density θ_J(I5 + X5) = 0.7336(3) among all of the analyzed ones. When a mixture consists of k-mers of different lengths, the jamming density fraction of the shorter k-mer is always larger than the fraction of the longer one.

The fractional jamming density of object L4, which gives the higher jamming densities in combination with other objects of the same size, is always larger than the fractional jamming density of the other object making the mixture. On the other hand, the fractional jamming density of object P4, which is the shape with the worst fitting capabilities when combined with objects of the same length, is almost always less than the fractional jamming density of the other component. The only exception is the combination with the k-mer ($k = 4$). As far as the mixtures of objects of size $n = 5$ are concerned, the fractional jamming density of L45 is always larger than the fractional jamming density of the other mixture component. Object X5, with the worst fitting

capabilities, has lower fractional jamming densities than any other examined object making the mixtures.

Problems of three-dimensional RSA of mixtures of lattice animals are extremely complex and there are many factors that affect the jamming density. The results of the simulations suggest that the number of possible orientations of the object is connected to its fractional jamming densities in the mixtures. Namely, for a majority of the investigated mixtures, a component with a larger number of orientations m has a larger value of the fractional jamming density. An object with larger m has a greater number of possibilities for filling the small empty regions left in the late stages of deposition. However, there are some exceptions to this rule: (O4, P4), (O4, T4), (V5, Y5), (L5, J15), (L5, L15), (L5, Z5), (J15, Y5), (L15, Y5), and (Y5, Z5). They can be explained by the individual characteristics of the objects breaking the rule:

- Object P4 has the worst fitting characteristics of the objects covering four lattice sites and its number of $m = 8$ possible orientations is not enough to make its fractional jamming density prevail over the fractional jamming density of object O4 ($m = 3$).

- Objects T4 ($m = 12$) and Y5 ($m = 24$) have a site at their side that makes their fitting more difficult.

- Objects J15, L15, and Z5, with $m = 12$ possible orientations, exhibit larger fractional jamming packing than some objects with $m = 24$ possible orientations. Mutual feature of these objects is that they have two angled elements at their end, making them more convenient for packing.

4. Concluding remarks

We have performed extensive numerical simulations of the RSA of binary mixtures of lattice animals on a 3D cubic lattice. The kinetics of the process have been examined for a wide variety of shape combinations. The approach to the jamming limit was found to be exponential for all of the mixtures of lattice animals, as well as for the mixture components. In the case of single-object deposition, the relaxation time σ (equation (1)) has been found to be determined by the number m of possible different orientations of the lattice animals on a cubic lattice [45]. For the mixtures, the rapidity of the approach to the jamming limit was found to be determined by the component shape with a larger number of possible orientations m. The value of the relaxation time σ for a mixture is approximately twice the relaxation time for the pure component with larger m.

Jamming coverages for the mixtures were determined for a large number of combinations of lattice animals covering the same number of sites. For $n = 3$ and $n = 4$ it was easy to find all of these combinations. The number of different shapes rapidly increases with n, so the mixtures of $n = 5$ size objects were made for all combinations of twelve chosen objects ($\binom{12}{2} = 66$ mixtures). This set contains the k-mer, a number of planar objects, and a number of three-dimensional lattice animals. On the bases of these results we have drawn some conclusions, but due to the complexity of the object shapes, these rules do have some exceptions. As expected, there are many factors that affect the packing facilities of the lattice animals making the mixtures. Nevertheless, we can conclude that:

- Jamming limit for a great majority of the mixtures has larger values than θ_J for the single mixture components.

- Components with a larger number of possible orientations m are favored when packing with objects with a smaller m. This is a consequence of the fact that an object with larger m has a greater number of possibilities for filling the small empty regions left in the late stages of the process.

- Jamming density for a mixture of k-mers of two different lengths is always larger than θ_J for either of the components. When a mixture is made of k-mers of different lengths, the jamming density fraction of the shorter k-mer is always larger than the fraction of the longer one.

- Among the objects covering four lattice sites ($n = 4$) object L4 shows the best packing facilities with other objects, while object P4 has the worst fitting capabilities when combined with objects of the same size. The results for the examined objects covering five lattice sites show that objects L45 and T25 give the largest values of jamming densities combining with other examined objects. On the other hand, the results of the simulations show that object X5 as a component of the mixture causes the lowest jamming limits.

- presented results also suggest that k-mers have low fitting capabilities. On the contrary, lattice animals made by bending one end of a k-mer (L4), or made of two parts of a broken k-mer (L45, T25), have very good packing facilities when combined with other objects.

Taking into account a small number of papers related to the RSA in three dimensions, the presented results can be viewed as the initial steps in understanding of RSA of complex objects on 3D lattices. Future investigations could be focused on the RSA of polydisperse mixtures in 3D, or on the RSA on 3D lattices with quenched impurities.

Acknowledgments

References

[1] Bernal J D 1964 The Bakerian lecture, 1962. The structure of liquids *Proc. R. Soc.* A **280** 299–322
[2] Torquato S 2002 *Random Heterogeneous Materials: Microstructure and Macroscopic Properties* vol 16 (New York: Springer)
[3] Chaikin P M and Lubensky T C 2000 *Principles of Condensed Matter Physics* vol 1 (Cambridge: Cambridge University Press)
[4] Mehta A 1994 *Granular Matter: An Interdisciplinary Approach* (New York: Springer)
[5] de Gennes P G 1999 Granular matter: a tentative view *Rev. Mod. Phys.* **71** S374–82
[6] Aste T 2005 Variations around disordered close packing *J. Phys.: Condens. Matter.* **17** S2361–90
[7] Torquato S and Stillinger F H 2010 Jammed hard-particle packings: from Kepler to Bernal and beyond *Rev. Mod. Phys.* **82** 2633–72

[8] Gevertz J L and Torquato S 2008 A novel three-phase model of brain tissue microstructure *PLoS Comput. Biol.* **4** e1000152

[9] Purohit P K, Kondev J and Phillips R 2003 Mechanics of DNA packaging in viruses *Proc. Natl Acad. Sci. USA* **100** 3173–8

[10] Liang J and Dill K A 2001 Are proteins well-packed? *Biophys. J.* **81** 751–66

[11] Conway J H and Sloane N J A 1999 *Sphere Packings, Lattices and Groups* (New York: Springer)

[12] Cohn H and Elkies N 2003 New upper bounds on sphere packings: I *Ann. Math.* **157** 689–714

[13] Hales T 2005 A proof of the Kepler conjecture *Ann. Math.* **162** 1065–185

[14] Evans J W 1993 Random and cooperative sequential adsorption *Rev. Mod. Phys.* **65** 1281–329

[15] Zhang G and Torquato S 2013 Precise algorithm to generate random sequential addition of hard hyperspheres at saturation *Phys. Rev.* E **88** 053312

[16] Talbot J, Tarjus G and Viot P 2000 Adsorption–desorption model and its application to vibrated granular materials *Phys. Rev.* E **61** 5429–38

[17] Budinski-Petković Lj and Vrhovac S B 2005 Memory effects in vibrated granular systems: response properties in the generalized random sequential adsorption model *Eur. Phys. J.* E **16** 89–96

[18] Zuppa C, Ciacera M and Zgrablich G 1999 Cooperative sequential adsorption of k-mers on heterogeneous substrates *Langmuir* **15** 5984–9

[19] Adamczyk Z, Barbasz J and Zembala M 2007 Particle assembly on surface features (patterned surfaces) *Langmuir* **23** 5557–62

[20] Stojiljković D, Šćepanović J R, Vrhovac S B and Švrakić N M 2015 Structural properties of particle deposits at heterogeneous surfaces *J. Stat. Mech.* P06032

[21] Talbot J, Tarjus G, Van Tassel P R and Viot P 2000 From car parking to protein adsorption: an overview of sequential adsorption processes *Colloids Surf.* A **165** 287–324

[22] Anton-Sanchez L, Bielza C, Merchán-Pérez A, Rodríguez J-R, DeFelipe J and Larranaga P 2014 Three-dimensional distribution of cortical synapses: a replicated point pattern-based analysis *Front. Neuroanat.* **8** 85

[23] Manna S S and Svrakic N M 1991 Random sequential adsorption: line segments on the square lattice *J. Phys. A: Math. Gen.* **24** L671–6

[24] Budinski-Petković Lj and Kozmidis-Luburić U 1997 Jamming configurations for irreversible deposition on a square lattice *Physica* A **236** 211–9

[25] Budinski-Petković Lj and Kozmidis-Luburić U 1997 Random sequential adsorption on a triangular lattice *Phys. Rev.* E **56** 6904–8

[26] Budinski-Petković Lj, Lončarević I, Dujak D, Karač A, Šćepanović J R, Jakšić Z M and Vrhovac S B 2017 Particle morphology effects in random sequential adsorption *Phys. Rev.* E **95** 022114

[27] Cooper D W 1988 Random-sequential-packing simulations in three dimensions for spheres *Phys. Rev.* A **38** 522–4

[28] Talbot J, Schaaf P and Tarjus G 1991 Random sequential addition of hard spheres *Mol. Phys.* **72** 1397–406

[29] Torquato S, Uche O U and Stillinger F H 2006 Random sequential addition of hard spheres in high Euclidean dimensions *Phys. Rev.* E **74** 061308

[30] Sherwood J D 1990 Random sequential adsorption of lines and ellipses *J. Phys. A: Math. Gen.* **23** 2827–33

[31] Cieśla M, Pajak G and Ziff R M 2016 In a search for a shape maximizing packing fraction for two-dimensional random sequential adsorption *J. Chem. Phys.* **145** 044708

[32] Vigil R D and Ziff R M 1990 Kinetics of random sequential adsorption of rectangles and line segments *J. Chem. Phys.* **93** 8270–2

[33] Kasperek W, Kubala P and Cieśla M 2018 Random sequential adsorption of unoriented rectangles at saturation *Phys. Rev.* E **98** 063310

[34] Cieśla M and Karbowniczek P 2015 Random sequential adsorption of starlike particles *Phys. Rev.* E **91** 042404

[35] Aleksić B N, Švrakić N M and Belić M 2013 Kinetics of deposition of oriented superdisks *Phys. Rev.* E **88** 062112

[36] Viot P, Tarjus G, Ricci S M and Talbot J 1992 Random sequential adsorption of anisotropic particles: I. Jamming limit and asymptotic behavior *J. Chem. Phys.* **97** 5212–8

[37] Cieśla M and Kubala P 2018 Random sequential adsorption of cubes *J. Chem. Phys.* **148** 024501

[38] Cieśla M and Kubala P 2018 Random sequential adsorption of cuboids *J. Chem. Phys.* **149** 194704

[39] Cieśla M 2013 Continuum random sequential adsorption of polymer on a flat and homogeneous surface *Phys. Rev.* E **87** 052401

[40] Wang J-S and Pandey R B 1996 Kinetics and jamming coverage in a random sequential adsorption of polymer chains *Phys. Rev. Lett.* **77** 1773–6

[41] Lebovka N I, Karmazina N N, Tarasevich Y Y and Laptev V V 2011 Random sequential adsorption of partially oriented linear k-mers on a square lattice *Phys. Rev.* E **84** 061603

[42] Lebovka N I, Tarasevich Y Y, Dubinin D O, Laptev V V and Vygornitskii N V 2015 Jamming and percolation in generalized models of random sequential adsorption of linear k-mers on a square lattice *Phys. Rev.* E **92** 062116

[43] Tarasevich Y Y and Cherkasova V A 2007 Dimer percolation and jamming on simple cubic lattice *Eur. Phys. J.* B **60** 97

[44] García G D, Sanchez-Varretti F O, Centres P M and Ramirez-Pastor A J 2015 Random sequential adsorption of straight rigid rods on a simple cubic lattice *Physica* A **436** 558–64

[45] Lončarević I, Budinski-Petković Lj, Šćepanović J R, Jakšić Z M and Vrhovac S B 2020 Random sequential adsorption of lattice animals on a three-dimensional cubic lattice *Phys. Rev.* E **101** 012119

[46] Harris A B and Lubensky T C 1981 Connection between percolation and lattice animals *Phys. Rev.* B **23** 3591–6

[47] Conway A R and Guttmann A J 1995 On two-dimensional percolation *J. Phys. A: Math. Gen.* **28** 891–904

[48] Sykes M F and Glen M 1976 Percolation processes in two dimensions: I. Low-density series expansions *J. Phys. A: Math. Gen.* **9** 87–95

[49] Lunnon W F 1971 Counting polyominoes *Computers in Number Theory* ed A O L Atkin and B J Birch (New York: Academic) pp 347–72

[50] Gaunt D S, Sykes M F and Ruskin H 1976 Percolation processes in D-dimensions *J. Phys. A: Math. Gen.* **9** 1899–911

[51] Aleksandrowicz G and Barequet G 2009 Counting polycubes without the dimensionality curse *Discrete Math.* **309** 4576–83

[52] Jensen I 2001 Enumerations of lattice animals and trees *J. Stat. Phys.* **102** 865–81

[53] Redelmeier D H 1981 Counting polyominoes: yet another attack *Discrete Math.* **36** 191–203

[54] Lunnon W F 1972 Symmetry of cubical and general polyominoes *Graph Theory and Computing* ed R C Read (New York: Academic) pp 101–8

[55] OEIS Foundation Inc. 2019 Sequence A000162 *The On-Line Encyclopedia of Integer Sequences* ed N J A Sloane

[56] Švrakić N M and Henkel M 1991 Kinetics of irreversible deposition of mixtures *J. Phys. I France* **1** 791–5